Proceedings of the ASME 2020 International Design Engineering Technical Conference & Computers and Information in Engineering Conference
IMECE 202
August 16-19, 2020, St. Louis, USA

IDETC2020-22137

ERROR QUANTIFICATION IN DYNAMIC APPLICATIONS OF WEAKLY NONLINEAR TRANSDUCERS

Lautaro Cilenti *
Department of Mechanical Engineering
University of Maryland - College Park
College Park, Maryland 20742
Email: lcilenti@terpmail.umd.edu

Akobuije Chijioke
Mass and Force Group
National Institute of Standards and Technology
Gathersburg, Maryland 20878
Email: Ako.Chijioke@nist.gov

Nicholas Vlajic
Applied Research Laboratory
The Pennsylvania State University
University Park, Pennsylvania 16802
Email: nav5000@arl.psu.edu

Balakumar Balachandran
Department of Mechanical Engineering
University of Maryland - College Park
College Park, Maryland 20742
Email: balab@umd.edu

ABSTRACT

Characterization and quantification of dynamic measurements is an ongoing area of research in the metrological community, as new calibration methods are being developed to address dynamic measurement applications. In the development undertaken to date, one largely assumes that nominally linear transducers can be used with linear assumptions in deconvolution of the input from the response and in system identification. To quantify the errors that arise from these assumptions, in this article, the effects of weak nonlinearities in transducers that are assumed to behave linearly during dynamic excitations are studied. Specifically, a set of first-order and second-order systems, which can model many transducers with weak nonlinearities, are used to numerically quantify the systemic errors due to the linear assumptions underlying the deconvolution. We show through the presented results the evolution of different error metrics over a large parameter space of possible transducers. Additionally, an example of quantification of the errors due to linear assumptions in system identification is demonstrated by using a time-series sparse regression system identification strategy. It is shown that the errors generated from linear identification of a nonlinear transducer can counteract the systemic errors that arise in linear deconvolution when the linear system identification is performed in similar loading conditions. In general, the methodology and results presented here can be useful for understanding the effect of nonlinearity in single degree of freedom transient dynamics deconvolution and specifically in specifying certain metrics of errors in transducers with known weak nonlinearities.

INTRODUCTION

Dynamic calibrations and signal deconvolution for transducers are a major area of development in the metrology community over the past decade [1, 2]. The developed framework for evaluating measurement uncertainty relies on the principle of superposition [3]. However, this principle does not apply for finding a response of a nonlinear system. Hence, weak nonlinearities in transducers are a source of unaccounted error.

Much work has been done to analyze the effects of weak nonlinear terms on the system response when the system is subjected to harmonic forcing. As an example, it is mentioned that Nayfeh and Mook [4] have shown how the frequency response of

*Address all correspondence to this author.

a system with weak cubic nonlinearity can be approximated near a primary resonance, a sub-harmonic resonance, and a super-harmonic resonance by using perturbation methods. In general, these methods are meant for characterizing the responses of nonlinear systems subjected to a persistent excitation rather than a transient excitation such as an impulse. There are methods such as Volterra series based approaches, which have been used for determining the system response when subjected to an impulse input. Volterra series is a generalization of the convolution integral for nonlinear systems, and the Generalized Frequency Response Function (GFRF) may be considered as the equivalent one in the frequency domain [5].

A Volterra Series and GFRF consist of an infinite number of Volterra kernels; in practice they require truncation for actual application and can be computationally expensive for even low-order approximations [6, 7]. There has been previous work done on defining the generalized impulse response function for Gaussian impulses in applications related to the dynamic behavior of the economy [8]. In part due to the challenges encountered in identifying the effect of nonlinearity under arbitrary loading conditions, many transducers are designed to operate as linearly as possible, and in some cases, these transducers are subjected to nonlinear dynamics compensation strategies [9, 10].

Despite the efforts undertaken to date, transducers generally have some degree of nonlinearity in the responses which can lead to measurement errors. In this context, it is mentioned that we have found no previous work on quantification of the errors that arise in deconvolution when one assumes the responses of weakly nonlinear systems subjected to impulse loading conditions to be linear. Here, we use numerical methods to analyze a parameter space that we posit to be applicable to real transducers, and may be useful in quantifying the errors that arise due to the neglect of nonlinearities in nominally linear transducers.

In order to isolate the uncertainty due to the nonlinearity, other sources of potential measurement error are neglected. We assume noiseless measurements and that the dynamics of the system is exactly described by a first-order or second-order system, as shown in equation (1) and (2), respectively [11]. We focus primarily on transducers that are modeled as first-order systems, which can also be a suitable model for filtered certain second-order and higher systems. Some representative second-order system results are also included.

$$(a+\varepsilon_a)\frac{\mathrm{d}y}{\mathrm{d}t}+(\beta+\varepsilon_\beta)y+g(y)=F(t) \tag{1}$$

$$(a+\varepsilon_a)\frac{\mathrm{d}^2y}{\mathrm{d}t^2}+(\mu+\varepsilon_\mu)\frac{\mathrm{d}y}{\mathrm{d}t}+(\beta+\varepsilon_\beta)y+g(y,\frac{\mathrm{d}y}{\mathrm{d}t})=F(t) \tag{2}$$

In these equations, y represents the state of the systems and $F(t)$ represents the input. Errors in acquiring the parameters from imperfect system identification models are represented by the values with ε in the coefficients. The function $g(y)$ is used to represent the nonlinear terms. Systemic errors from possible additional linear terms are not shown here.

The coefficients in the nonlinear term $g(y)$ are assumed to be small, in keeping with the focus of this study on transducers that have been designed to exhibit near linear behavior. These equations are used to model the behavior of a nonlinear sensor and approximate the error in an inferred (deconvolved) input.

The rest of the paper is organized as follows: The analytical methodology that is used as a basis for the simulations is described in Section 2. The numerical methodology including useful metrics for quantifying time series errors in inferring (or deconvolving) the response inputs are presented in Section 3. Results from the numerical simulations are presented in Section 4. Finally, we present conclusions and remarks to close the article.

ANALYTICAL METHODOLOGY

First-Order Systems

Nondimensionalization In reducing the relevant parameter space for numerical study, the system can be represented in nondimensionalized form with the change of variables shown in equation (3). After using x as the new state variable and τ as the new time scale, equation (1) is transformed into equation (4).

$$t=\frac{a}{\beta}\tau, \quad y=\frac{1}{\beta}x \tag{3}$$

$$\frac{\mathrm{d}x}{\mathrm{d}\tau}+x+\tilde{g}(x)=\tilde{F}(\tau) \tag{4}$$

Equation (4) is the system in nondimensionalized form, where x represents the nondimensionalized state variable, and τ represents the nondimensionalized time. The function $\tilde{g}(x)$ represents the nondimensionalized nonlinear term, and $\tilde{F}(\tau)$ is an arbitrary input resulting from the nondimensionalization of x and τ. It was assumed in this nondimensionalization that ε is equal to zero; that is, the system parameters are known accurately.

Model-Based Linear Deconvolution We consider sensors that are accurately described by equation (4), and define a model-based linear deconvolution as evaluating the input from the output by using a linear differential equation with the same parameters as the nonlinear system.

$$\frac{\mathrm{d}\hat{x}}{\mathrm{d}\tau}+\hat{x}+\tilde{g}(\hat{x})=\hat{\tilde{F}}(\tau) \tag{5}$$

$$F_{\text{estimated}} = \frac{\mathrm{d}\hat{x}}{\mathrm{d}\tau} + \hat{x} \tag{6}$$

From Equation (5), it follows that for the input $\hat{\tilde{F}}(\tau)$, the system has the response or solution $\hat{x}$. The error in the estimated input can be quantified by the difference between the estimated input and the actual input.

$$F_{\text{actual}} \equiv \hat{F}(\tau) \tag{7}$$

$$e(\tau) \equiv |F_{\text{estimated}} - F_{\text{actual}}| = |-\tilde{g}(\hat{x})| \tag{8}$$

Modeling Nonlinearity The systems described in equation (1) can be used to represent any arbitrary nonlinear system whose form depends on a transducer's behavior. In this paper, we restrict attention to the nonlinearities represented by equation (9).

$$\tilde{g}(x) = \alpha_2 |x| x + \alpha_3 x^3 \tag{9}$$

The considered nonlinear terms are limited up to third order, as transducers are generally meant to be as linear as possible. The higher powers of nonlinearity are assumed to be small. This general function $g(x)$ will be adapted as necessary by setting the coefficients of nonlinearities that are not present in a particular system to zero.

Additional Error From System Identification It is of practical interest to consider the errors that arise when linear system identification is used to construct a linear model of a nonlinear transducer. So far it has been assumed that the parameter ε is zero, meaning the parameters are the same in the linear model as in the true nonlinear system. This assumption is valid when nonlinear system identification has been used to generate the parameters for a system described by these models and where the system identification measurement errors are small. In the practical scenario wherein the system model is constructed from linear system identification, ε will include a component due to the ignored or unidentified nonlinearity during the system identification. Neglecting other sources of errors, we assign the value ε_o to ε. The parameter ε_o is zero when using nonlinear system identification for a nonlinear system and nonzero in general when using linear system identification for a nonlinear system.

When ε_o is nonzero, equation (8) is only valid approximately. This is further developed as follows: The actual nonlinear system has ε equal to zero and is described in nondimensionalized form by equation (4).

Alluding here to equation (1) which includes errors in the identified system parameters, in an application where the user has assumed the system to be linear and performed a noise free linear system identification, the corresponding model has nonzero $\varepsilon = \varepsilon_o$. This linear model is described by equation (10), where $\rho_n = \varepsilon_{n,o}/n$.

$$(1+\rho_a) a \frac{\mathrm{d}y}{\mathrm{d}t} + (1+\rho_\beta)\beta y = F(t) \tag{10}$$

In nondimensionalization of the linear system, the change of variables also takes the form shown in equation (3). The corresponding nondimensionalized versions of equation (10) is shown as equation (11).

$$(1+\rho_a)\frac{\mathrm{d}x}{\mathrm{d}\tau} + (1+\rho_\beta)x = \tilde{F}(\tau) \tag{11}$$

After substituting the particular solution $\hat{x}$ to obtain $F_{\text{estimated}}$ in equation (11) and taking the difference with F_{actual}, one obtains $e(\tau)$. Taking into account the ε_o error, equation (8) is replaced by equation (12).

$$e(\tau) \equiv |F_{\text{estimated}} - F_{\text{actual}}| = |-\tilde{g}(\hat{x}) + \xi(\tau)| \tag{12}$$

$$\xi(\tau) = \rho_a \frac{\mathrm{d}\hat{x}}{\mathrm{d}\tau} + \rho_\beta \hat{x} \tag{13}$$

The case where all $\rho = 0$ corresponds to the case where there is no nonlinearity. Also $\rho = 0$ for the case of perfect nonlinear system identification, and in which case equation (12) is equivalent to equation (8).

In this analysis, the type of nonlinearity or magnitude of the nonlinearity itself has not been considered. In a practical application, the type and magnitude of nonlinearity will determine the magnitudes of ρ.

Magnitude of System Identification Error, ρ At this point, it is unclear as to how large ρ can be for a particular nonlinearity. Since it is possible that (13) will be of the same magnitude as $\tilde{g}(\hat{x})$ for weak nonlinearities, it is necessary to understand how ρ changes with the nonlinearity to understand the applicability of this methodology in applications where nonlinear system identification is not performed. To quantify the magnitude of ρ for a particular nonlinearity and forcing amplitude, we selected a system identification methodology based on Kutz and colleagues' nonlinear identification of governing equations using sparse regression [12]. This methodology is meant to serve

only as an example, as it is likely that other linear system identification strategies will result in different errors in the parameters.

In nonlinear identification carried out with the method of Kutz and colleagues, a simulated nonlinear output, $\hat{x}$ from equation (4), is used to generate a matrix A of candidate nonlinear functions as shown in equation (14). Each row of the matrix corresponds to a time step of the discrete $\hat{x}$ and each column is a nonlinear transformation of $\hat{x}$ in terms that are candidates for the nonlinear model.

$$A_{nl} = \begin{pmatrix} \vdots & \vdots & \vdots & \vdots \\ \hat{x} & |\hat{x}|\hat{x} & \hat{x}^3 & \hat{\tilde{F}} \\ \vdots & \vdots & \vdots & \vdots \end{pmatrix} \tag{14}$$

We use this methodology while ignoring the nonlinear terms, allowing the regression to optimize the linear parameters to the nonlinear trajectory $\hat{x}$. A matrix is generated with only the terms in the linear differential equation as shown in equation (15).

$$A_l = \begin{pmatrix} \vdots & \vdots \\ \hat{x} & \hat{\tilde{F}} \\ \vdots & \vdots \end{pmatrix} \tag{15}$$

$$A_l \omega_l = \hat{x}_{dot} \tag{16}$$

In equation (16), $\hat{x}_{dot}$ is the time derivative of $\hat{x}$ computed by using the central difference formula, and ω_l is a vector of weights optimized for the governing equation that generated $\hat{x}$. After solving equation (16) with a solver that promotes sparsity, one obtains weights, ω_l, and generates equation (17).

Equation (18) is equivalent to (11). Comparing equation (17) to equation (18), we define equations (19) and (20).

$$\hat{x}_{dot} - \omega_l(1)\hat{x} = \omega_l(2)\hat{\tilde{F}} \tag{17}$$

$$\frac{\mathrm{d}x}{\mathrm{d}\tau} + \frac{(1+\rho_\beta)}{(1+\rho_a)}x = \frac{1}{(1+\rho_a)}\tilde{F} \tag{18}$$

$$\omega_l(1) \equiv \frac{-(1+\rho_\beta)}{(1+\rho_a)} \tag{19}$$

$$\omega_l(2) \equiv \frac{1}{(1+\rho_a)} \tag{20}$$

From equations (19) and (20), we derive ρ_a and ρ_b as shown in equation (21).

$$\rho_a = \frac{1}{\omega_l(2)} - 1, \quad \rho_b = -\omega_l(1) \times (1+\rho_a) - 1 \tag{21}$$

The ρ values obtained following this methodology can be used to quantify $e(\tau)$ as shown in equation (12).

Second-Order Systems

Here, we consider the second-order systems described by equation (2). The analysis described in this section follows along the same lines as that presented for the first-order systems and will be presented in condensed form.

The nondimensional version of the second-order system uses the change of variables in equation (22) to generate equation (23) from equation (2).

$$t = \sqrt{\frac{a}{\beta}}\tau, \quad y = \frac{1}{\beta}x, \quad \delta = \frac{\mu}{\sqrt{a\beta}} \tag{22}$$

$$\frac{\mathrm{d}^2x}{\mathrm{d}\tau^2} + \delta\frac{\mathrm{d}x}{\mathrm{d}\tau} + x + \tilde{g}(x, \frac{\mathrm{d}x}{\mathrm{d}\tau}) = \tilde{F}(\tau), \tag{23}$$

The parameter δ represents the nondimensionalized linear damping coefficient. The nonlinear terms in the second-order systems are described with $\tilde{g}(x, \frac{\mathrm{d}x}{\mathrm{d}\tau})$ that includes the lower order nonlinear velocity terms as shown in equation (24).

$$\tilde{g}(x, \frac{\mathrm{d}x}{\mathrm{d}\tau}) = \alpha_2|x|x + \alpha_3x^3 + \gamma_1 x\frac{\mathrm{d}x}{\mathrm{d}\tau} + \gamma_2\frac{\mathrm{d}x}{\mathrm{d}\tau}\left|\frac{\mathrm{d}x}{\mathrm{d}\tau}\right| \tag{24}$$

Following a similar approach as that for the first-order systems, the error, $e(\tau)$, can be calculated by taking the difference between an actual input and an estimated input calculated by applying the output of the nonlinear system, $\hat{x}$, to the linear system shown in equation (26).

$$\frac{\mathrm{d}^2\hat{x}}{\mathrm{d}\tau^2} + \delta\frac{\mathrm{d}\hat{x}}{\mathrm{d}\tau} + \hat{x} + \tilde{g}(\hat{x}, \frac{\mathrm{d}\hat{x}}{\mathrm{d}\tau}) = \hat{\tilde{F}}(\tau) \tag{25}$$

$$F_{\text{estimated}_2} = \frac{\mathrm{d}^2\hat{x}}{\mathrm{d}\tau^2} + \delta\frac{\mathrm{d}\hat{x}}{\mathrm{d}\tau} + \hat{x} \tag{26}$$

$$F_{\text{actual}} \equiv \hat{F}(\tau) \tag{27}$$

$$e(\tau) \equiv \left|F_{\text{estimated}_2} - F_{\text{actual}}\right| = \left|-\tilde{g}(\hat{x}, \frac{\mathrm{d}\hat{x}}{\mathrm{d}\tau})\right| \tag{28}$$

Note that the definition of $e(\tau)$ is in the same spirit for the second-order systems as that for the first-order systems.

Errors caused by nonlinearity in system identification can be quantified in a similar manner for the second-order systems as for the first order systems, but we do not do so here.

SIMULATION METHODOLOGY

Numerical Methods

Numerical integration of differential equations (4) and (23) was performed by using the Dormand-Prince method with a relative tolerance of 10^{-8} and an absolute tolerance of 10^{-8}. In order to obtain estimated F, the derivatives of the solutions were calculated by using a central difference formula. Since, in the Dormand-Prince method, one does not attempt to minimize errors in the discrete derivative (relevant especially when discontinuities are present), the simulations were forced to run with step sizes smaller than or equal to h_{max}. The value of h_{max} was fixed to 0.01 based on visual inspection of convergence while minimizing simulation run-time. The simulations ran with different values of the parameters α_2, α_3, γ_1, and γ_2 for the nonlinearities given in equations (9) and (24). Only one nonlinear term was nonzero in a given simulation; combinations of nonlinearities were not studied. The input, $\tilde{F}(\tau)$, was a Gaussian envelope impulse described by equation (29) generated from the SciPy Python library [13], in which amplitude A and duration $\Delta\tau$ were varied.

$$\tilde{F}(\tau) = Ae^{C_1\tau^2}, \quad C_1 = -\frac{14.288}{(\Delta\tau)^2} \tag{29}$$

For finding the parameter space that generates a prescribed error due to nonlinearity, we ran the simulations by using an iterative solver based on Newton's method to find the input amplitude, A, that generates a prescribed error for a fixed magnitude of the nonlinear coefficient. Newton's method was automated to stop at convergence with thresholds of at most 10 % the magnitude of the prescribed error.

The open source Scikit-learn lasso regression module [14] available on python was used to perform sparse regression in implementing Kutz's and colleagues' system identification methodology. A small regularizer in lasso regression promotes sparsity. The regularizing parameter, λ, was fixed to 10^{-6}. The regression module was also configured to run a maximum of 10^5 iterations or to stop at convergence tolerances of 10^{-6}. When performing nonlinear system identification as a control, this configuration kept the errors in the weights of the system identification methodology at around 0.1 % when used with simulated input amplitudes greater than 10 and smaller than 10^4. The additional systemic error generated from ignoring nonlinear terms in the linear identification regression are reported in the results.

Error Metrics

Since the response of the system and its errors are a function of time for dynamic loading, some useful metrics for dynamic error quantification are presented within this section. When the maximum error due to nonlinearity is of interest, the maximum point by point error can be quantified by using equation (30).

$$M_1 \equiv e_{\max} = \frac{max(|e(\tau)|)}{max(|F_{\text{estimated}}(\tau)|)} \tag{30}$$

When the integrated input is of interest, the relevant errors can be quantified by using equation (31).

$$M_2 \equiv e_{\text{integral}} = \frac{\int_0^{\tau_f} e(\tau)d\tau}{\int_0^{\tau_f} F_{\text{estimated}}(\tau)d\tau} \tag{31}$$

In equation (31), the denominator represents the integral of estimated F with respect to time and the numerator represents the integral of the error in estimated F due to nonlinearity with respect to time. The parameter $\tau_f >> \Delta\tau$, meaning that the integration continues until the transient response due to an input of duration $\Delta\tau$ has died out.

When the peak input is of interest, the error can be quantified by equations (32)-(34).

$$\tau_{\max 1} = \text{argmax}(|F_{\text{actual}}(\tau)|) \tag{32}$$

$$\tau_{\max 2} = \text{argmax}(|F_{\text{estimated}}(\tau)|) \tag{33}$$

$$M_3 = e_{\text{PeakRatio}} = \frac{|F_{\text{actual}}(\tau_{\max 1}) - F_{\text{estimated}}(\tau_{\max 2})|}{|F_{\text{estimated}}(\tau_{\max 2})|} \tag{34}$$

The denominator in equation (34) represents the peak estimated input, and the numerator represents the difference in peaks between the actual input and the estimated input.

The metrics are applied in post-processing of simulations in parameter space of input amplitude, A, input duration, $\Delta\tau$, and nonlinearity coefficients from equations (9) and (24). They can be used to obtain uncertainty estimates when an inferred peak or integrated input is known by multiplying the error ratios with the experimental inferred input values.

RESULTS

First-Order System Results

Simulations of first-order systems with quadratic or cubic nonlinearity subjected to a gaussian impulse were conducted. From the response, an inferred linearly deconvolved input was calculated by neglecting the nonlinear term. An inferred input from a nonlinear system with a relatively large cubic nonlinear term compared to the actual input is shown in Fig. 1. The three error metrics are evaluated in post-processing. From Fig. 2, one can observe the parameter space of forcing amplitude and nonlinearity coefficient where the errors at the peaks (equation (34)) are 10 % the inferred input amplitude. We note that the cubic nonlinearity has a slope of $-\frac{1}{2}$ and the quadratic nonlinearity has a slope of -1 in the log space of input amplitude A and nonlinearity coefficient. These slopes are consistent for the three different error metrics and for different $\Delta\tau$. Lines corresponding to error at the peak (Metric 3: equation (34)) of 1 %, 10 %, 20 %, 50 %, and 90 % for a cubic nonlinearity are shown in Fig. 3. It can be inferred from this graph that transducers that are used with input amplitudes smaller than the 1 % line yield error metric values smaller than 1 % when used to infer an input. We show in Fig. 4 the vertical shift in the lines for the three different error metrics

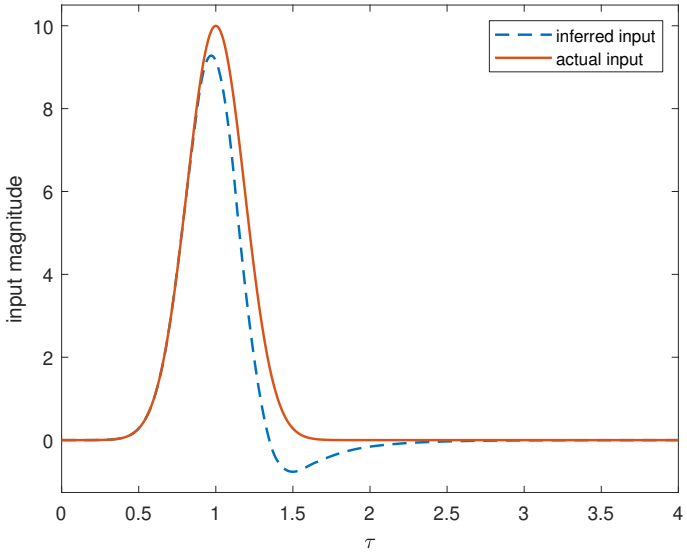

FIGURE 1. Inferred input compared to the actual input for a nonlinear system with $\tilde{g}(x) = 0.1x^3$

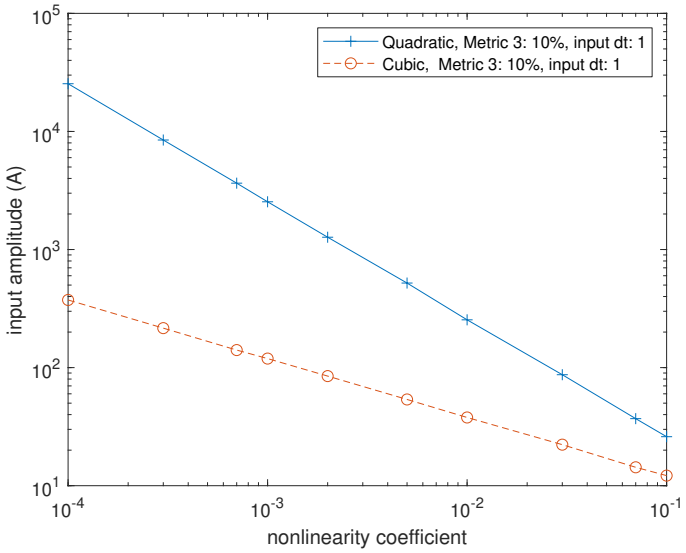

FIGURE 2. Gaussian input amplitude plotted with nonlinearity coefficient for quadratic ($|x|x$) and cubic (x^3) nonlinear terms that produce error at peak metric values of 10 %. The errors are smaller than 10 % in the parameter space below the lines.

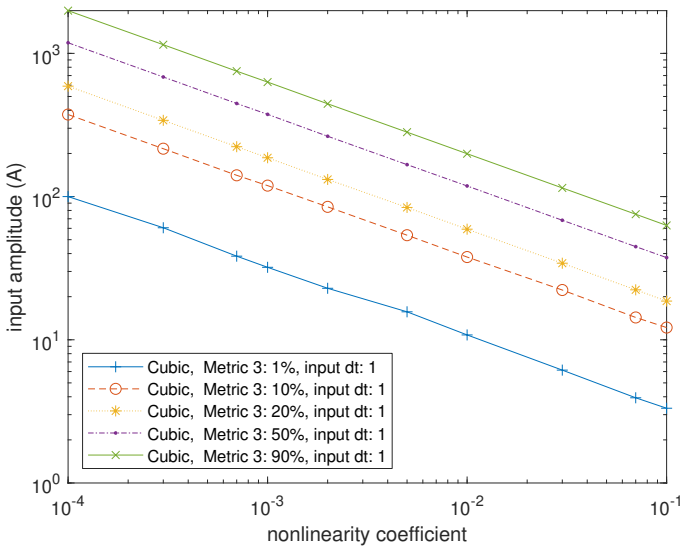

FIGURE 3. Gaussian input amplitude plotted with nonlinearity coefficient for cubic (x^3) nonlinear terms that produce errors of varying magnitude.

for a cubic nonlinearity with a fixed metric value of 10 %. Metric 1, representing the maximum error between the inferred input and the actual input (equation (30)) yields 10 % errors at lower input amplitudes than metric 2, the error at the peaks (equation (34)). It can be inferred from this observation that the maximum error in deconvolution does not occur at the inferred peak; this

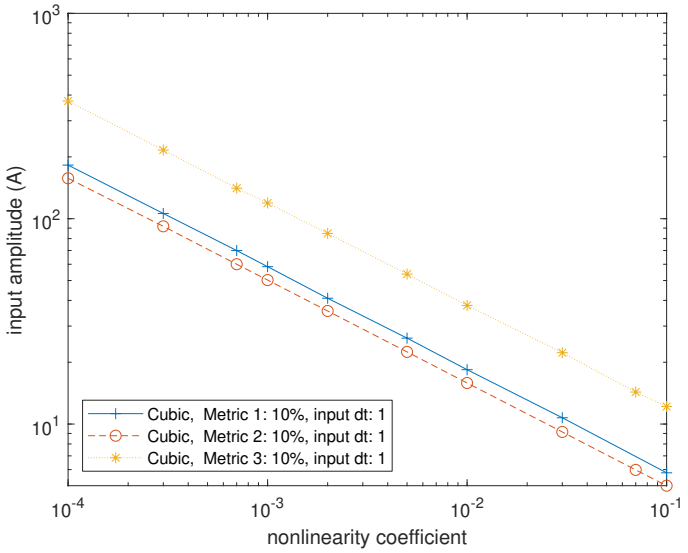

FIGURE 4. Gaussian input amplitude plotted with nonlinearity coefficient for cubic (x^3) nonlinear terms that produce error magnitudes of 10 % for the three different error metrics.

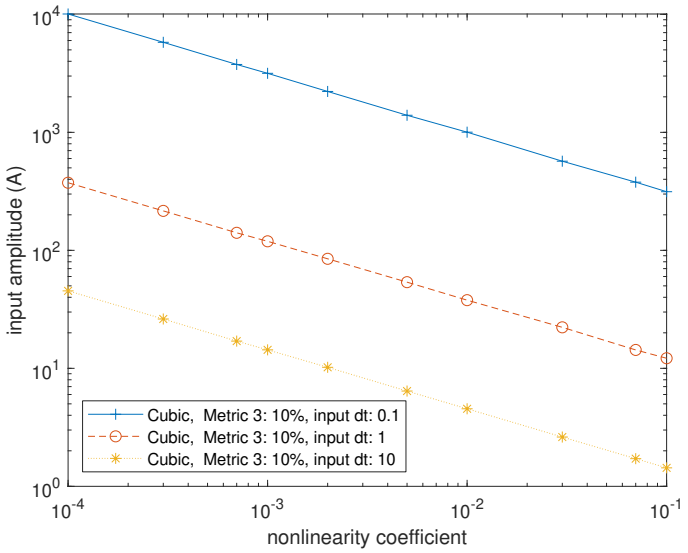

FIGURE 5. Gaussian input amplitude plotted with nonlinearity coefficient for cubic (x^3) nonlinear terms that produce error magnitudes of 10 % for metric 3 with three different input durations.

can also be observed in the example of Fig. 1. The vertical shift in the lines for three different $\Delta\tau$ with a fixed metric value of 10 % are shown in Fig. 5. We note that $\Delta\tau = 0.1$ corresponds to the largest bandwidth of excitation in this study. It is expected that the Metric 1 and 3 lines will converge to the static case at the limit $\Delta\tau \to \infty$. From observations made in figs. 2 to 5, we generated Table 1 and equation (35) as an interpolating model

TABLE 1. Parameters m_1, m_2, and b can be used in equation (35) to approximate the error value for a particular system. Here, 1^* is bound as $1 > 1^* \geq 0.995$.

Δt	Metric	x^3				$\lvert x\rvert x$			
		m_1	m_2	b	R^2	m_1	m_2	b	R^2
0.1	1	-0.5	0.49	2.21	0.90	-1	1.40	3.08	1^*
0.1	2	-0.5	0.91	2.17	0.95	-1	2.37	2.97	0.98
0.1	3	-0.5	0.68	2.71	0.99	-1	1.22	3.51	1^*
1	1	-0.5	0.73	0.99	1^*	-1	1.30	1.27	1^*
1	2	-0.5	0.68	0.92	0.99	-1	1.48	1.22	0.99
1	3	-0.5	0.64	1.2	0.99	-1	1.20	1.6	1^*
10	1	-0.5	0.61	0.26	0.99	-1	1.22	0.33	1^*
10	2	-0.5	0.65	0.43	0.98	-1	1.26	0.49	1^*
10	3	-0.5	0.6	0.29	0.99	-1	1.18	0.37	1^*

for the included figures and those not included. This can be used to generate an approximate error metric value corresponding to a nonlinear coefficient, α, and impulse amplitude, A.

$$M(\alpha,A) = 100 \times 10^{\left(\frac{\log_{10}(A) - m_1\log_{10}(\alpha) - b}{m_2}\right)} \tag{35}$$

As shown in Table 1, the parameters m_1, m_2, and b have R^2 values close to 1. This indicates that the linear regression in the interpolating model fit the data well. In the parameter range shown in the included figures, the interpolating model is accurate within a factor of 2.

First-Order System Identification Error

After using Kutz's and colleagues' system identification from data approach, $e(\tau)$ was recalculated considering the error in linear system identification of a nonlinear system. The new $e(\tau)$ from equation (12) produces new metric values and shifts metric lines as shown in Fig. 6. One can observe from Fig. 6 that the metric lines of 10 % that include nonzero ρ error occur at higher forcing amplitudes than the original system. One way to understand this behavior is to note that the resulting sign of ρ has the effect of counteracting the negative $\tilde{g}(\hat{x},\tau)$ in $e(\tau)$; a smaller $e(\tau)$ yields a smaller metric value resulting in higher input amplitude or nonlinear coefficients to produce the same error. A more intuitive way of understanding the effect is to observe that the optimization of the linear parameters to the nonlinear data by using linear system identification reduced the error between the linear inferred input and the actual input because it was optimized to do so through an adjustment in the linear parameters during regression. As shown in Fig. 7, the same trend occurs for all three metrics at 10 %. We note at this point that the ρ values were obtained with linear system identification at same input amplitude that was used for the inferring procedure. Unlike in the

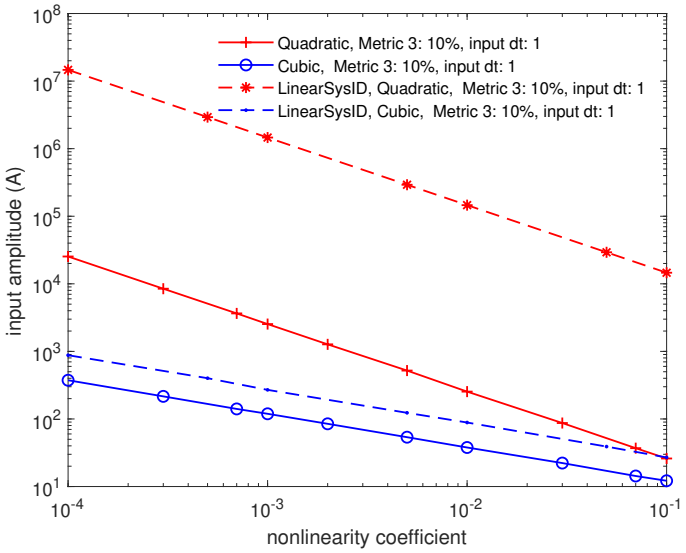

FIGURE 6. Gaussian input amplitude plotted with nonlinearity coefficient for quadratic ($|x|x$) and cubic (x^3) nonlinear terms that produce error at peak metric values of 10 %. The plot compares the actual nonlinear system results with the results of considering the ρ_a and ρ_b errors generated from performing linear system identification on the nonlinear system.

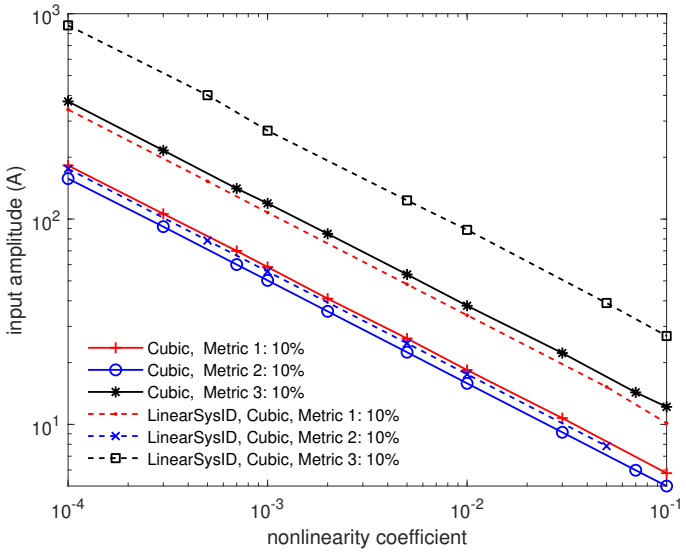

FIGURE 7. Gaussian input amplitude plotted with nonlinearity coefficient for cubic (x^3) nonlinear term that produce error at peak metric values of 10 %. The plot compares the actual nonlinear system results with the results of considering the ρ_a and ρ_b errors generated from performing linear system identification on the nonlinear system for the three metrics.

case of nonlinear system identification of the parameters, the optimization of the parameters by using linear system identification is only valid at the amplitude of the input used for generating $\hat{x}$ prior to regression. With this in mind, we show the contour plots in Fig. 8 and 9 which illustrate how ρ changes in the parameter space.

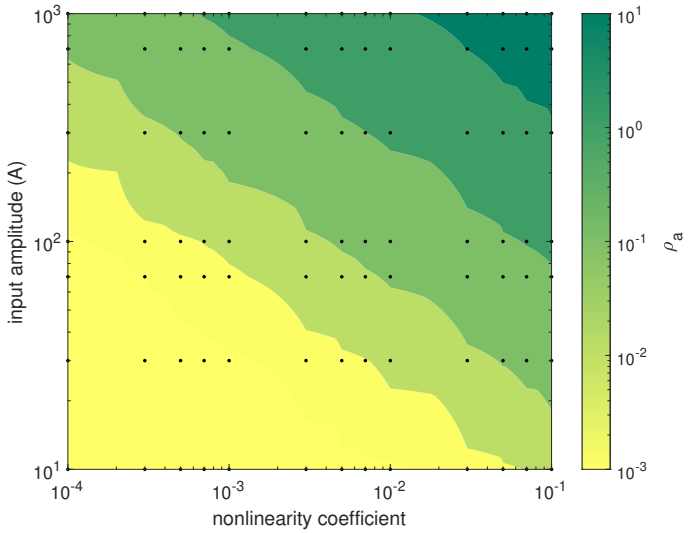

FIGURE 8. ρ_a magnitude in parameter space of input amplitude and nonlinearity coefficient for system with cubic nonlinearity. Simulated points are shown as black dots.

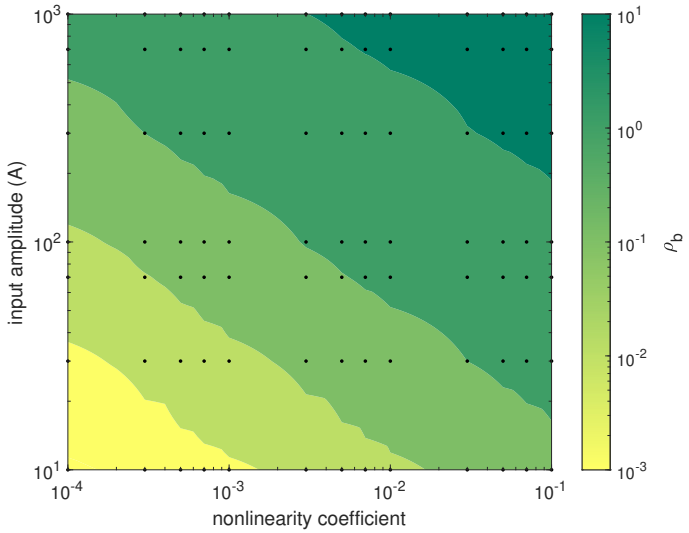

FIGURE 9. ρ_b magnitude in parameter space of input amplitude and nonlinearity coefficient for system with cubic nonlinearity. Simulated points are shown as black dots.

The parameter space shown in Fig. 8 and 9 contains only positive values of ρ. For larger input amplitudes and lower input amplitudes than presented, the sparse regression failed to con-

verge. This is likely a direct result of the tight tolerances and small regularizer used for lasso regression, but may be related to the ability to identify a nonlinear system through linear identification when excited by very small amplitudes or very large amplitudes.

Second-Order System Results

From the responses of second-order systems with nonlinearities subjected to a Gaussian impulse an inferred linearly deconvolved input was calculated by neglecting the nonlinear term. The inferred input for four different types of nonlinearities are shown in Fig. 10.

From Fig. 10 and explorations of the parameter space for the second-order system, it can be qualitatively observed that the nonlinearity does not have a large effect on the peak inferred input. However, the nonlinearity modulates the frequency of the response and generates transient oscillations in the inferred input after the first peak that decay at rates depending on the linear or nonlinear damping. Furthermore, as shown in Fig. 11, for higher forcing amplitudes of the same nonlinear systems, the peak inferred inputs can occur at the second peak of oscillation. This indicates strongly nonlinear behavior and transducers that exhibit this behavior would not be considered nominally linear.

Based on these qualitative observations, we note that Metric 3 which quantifies errors at the peaks is of small magnitude for the second order system until there is such strongly nonlinear behavior that the second peak can be larger than the first peak. Furthermore, due to the contribution of transient oscillations after the first peak in highly nonlinear behavior, the error metrics can be highly dependent on the damping ratio of the system.

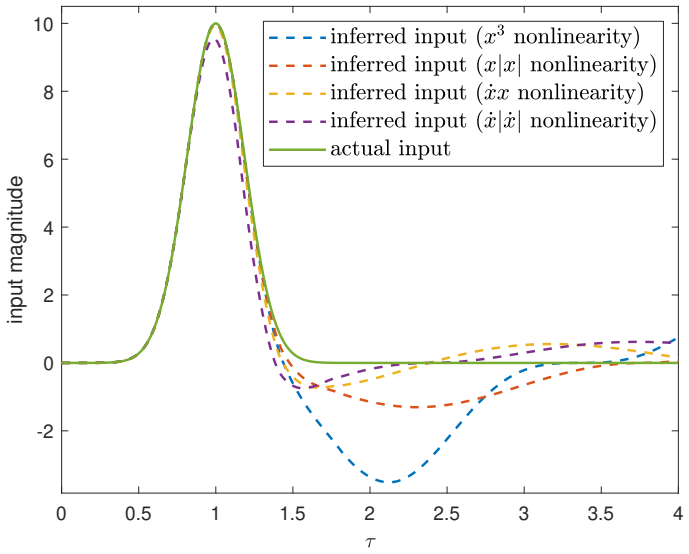

FIGURE 10. Inferred inputs compared to the actual input for nonlinear second order systems with $\tilde{g}(x, \frac{dx}{d\tau})$ of $0.1x^3$, $0.1x|x|$, $0.1x\frac{dx}{d\tau}$, and $0.1\frac{dx}{d\tau}\left|\frac{dx}{d\tau}\right|$ and damping term $\delta = 0.2$.

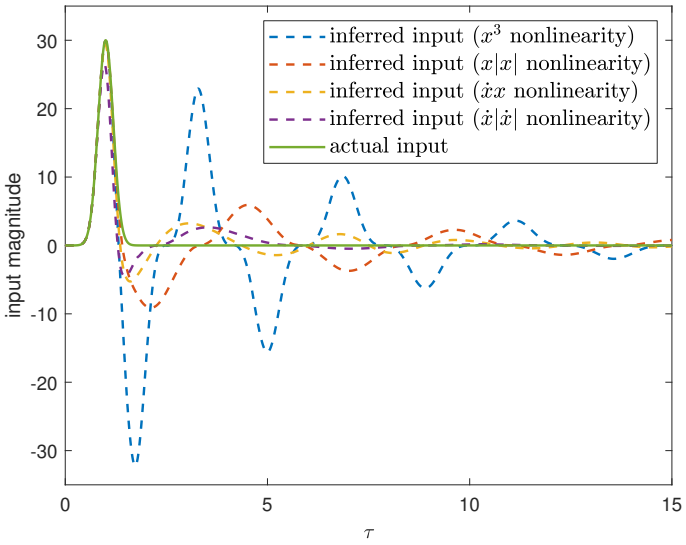

FIGURE 11. Inferred inputs compared to the actual input for nonlinear second order systems with $\tilde{g}(x, \frac{dx}{d\tau})$ of $0.1x^3$, $0.1x|x|$, $0.1x\frac{dx}{d\tau}$, and $0.1\frac{dx}{d\tau}\left|\frac{dx}{d\tau}\right|$ and damping term $\delta = 0.2$. Notice the second peak can be higher than the first for the inferred input.

We limit the scope of the analysis of the second order system in this paper to a few examples. From Fig. 12, one can observe the parameter space by which errors at the peaks remain below 1 ± 0.1 % for the four different nonlinear terms. As shown in Fig. 13 for systems with cubic nonlinearity the error rises quickly after it has reached 1 %. This occurs because at the 1 % line for the cubic nonlinearity, the second peak is larger than the first peak and it continues to grow with increasing input amplitudes. One may take away from this nonetheless that certain nonlinearities will produce errors smaller that 1 % up to the point they are so large that they are producing high second peaks in the inferred input.

We show in Fig. 14 how Metric 2, the error in the integral of the inferred input, decreases with increasing damping ratio for a system with the nonlinear function $g(x, \frac{dx}{d\tau}) = 0.01x^3$. This behavior is also observed for the other three nonlinear terms and also generates lower Metric 1 and Metric 2 errors with greater damping as it takes higher input amplitudes and nonlinear coefficients to generate high oscillations after the first inferred peak.

Finally we also show an example in Fig. 15 where changes to the excitation duration for the second order system shifts the error lines vertically as in the first order system. This is most likely due to the corresponding change in excitation momentum when the excitation amplitudes are held constant but the excitation duration is changed.

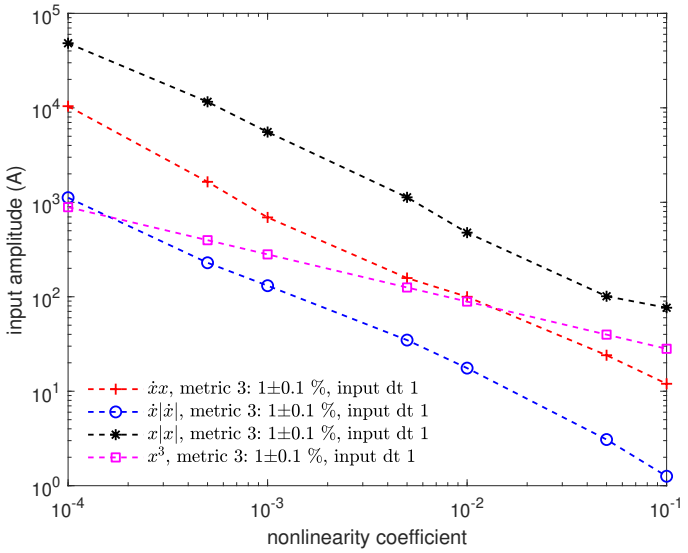

FIGURE 12. Error at the peaks of 1 ± 0.1 % between inferred input and actual input for four different nonlinear terms in a second-order systems with damping ratio $\delta = 0.2$ excited by a one second pulse.

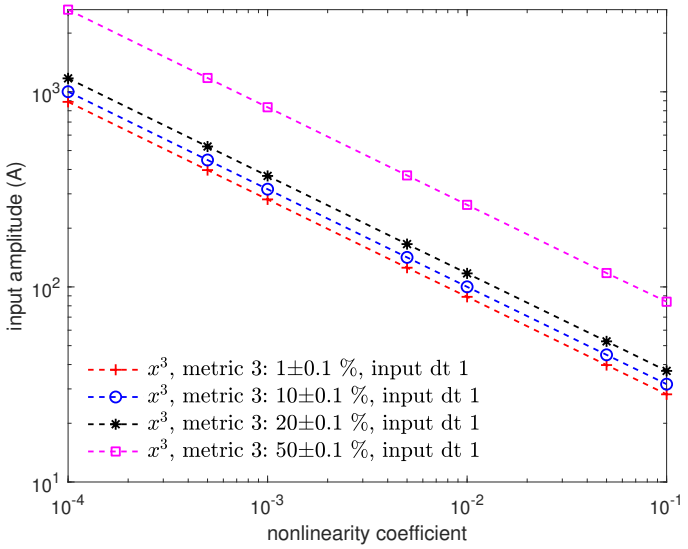

FIGURE 13. Error at the peaks between inferred input and actual input for cubic nonlinearity in second-order systems with damping ratio $\delta = 0.2$ excited by a one second pulse.

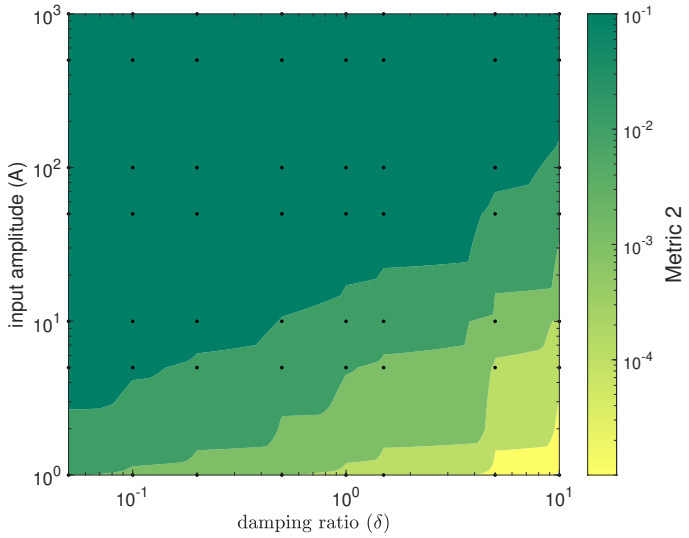

FIGURE 14. Filled contour of integral error ratio (metric 2) as a function of damping ratio and input amplitude for a fixed nonlinearity, $0.01x^3$.

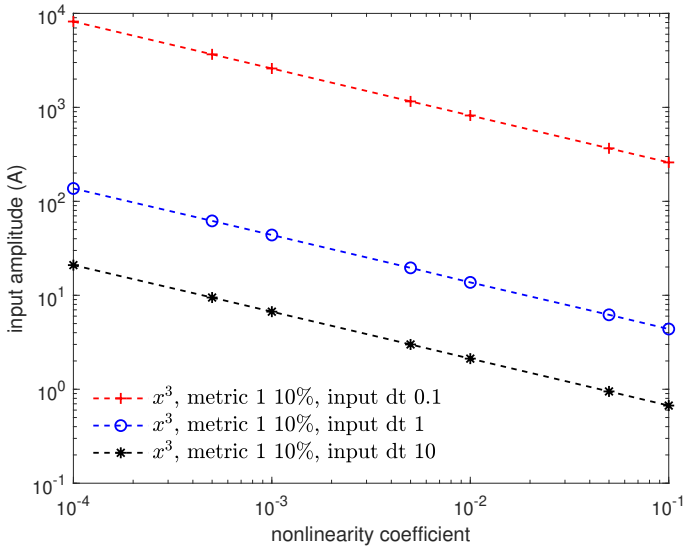

FIGURE 15. Maximum error between inferred input and actual input for three different bandwidths of excitations of a second order system with cubic nonlinearity and damping ratio $\delta = 0.2$.

DISCUSSION

A novel methodology for quantifying errors in the decovolution process in transducers, which can be modeled as first- or second-order systems is presented within the article. This methodology is not limited to nominally linear transducers. Here, the lower order nonlinear terms more prevalent in weakly nonlinear systems are considered. We also present error metrics that may be useful in quantifying errors in measurements with nominally linear transducers. Through simulations, we highlight the variations of the error metrics in a space of weak nonlinear coefficients. If upper bounds to the nonlinear coefficients and the input amplitudes for a transducer are known, then upper bounds to the error metrics can be estimated. Furthermore, we provide an interpolating function for estimating errors in deconvolution over the parameter space that was studied here.

We present a simple and novel methodology for quantifying the error that arises in ignoring the nonlinearity in a transducer during system identification. Through simulations, we show that using this approach, in first-order systems within the parameter space of this study, errors due to system identification can counter the errors in deconvolution by optimizing the inferred input to the actual input by using the linear parameters. A metrologist may be interested in this effect, noting certain linear calibration methods performed near measuring conditions for a nonlinear sensor may help diminish unaccounted errors in linear deconvolution.

For the second-order systems, we also present some examples where the errors in the second-order system are observed as transient oscillations after the first peak and decrease with higher linear damping ratios.

The parameter space studied is not comprehensive for nonlinear systems in general or nominally linear transducers. Additionally, only Gaussian impulses were explored and for only three limited bandwidths. Furthermore, the effects of noise were not considered in the methodology and simulations.

It would be interesting in future studies to compare this methodology and the associated results to results from deconvolution algorithms, to evaluate the extent to which real transducers fall within the parameter space considered here, and to test the methodology experimentally through real or representative transducers.

ACKNOWLEDGMENT

Partial support received for this work through the Non-Academic Research Internship for Graduate Students (INTERN) program provided by the U. S. National Science Foundation through Grant No. CMMI 1760366 is gratefully acknowledged.

Lautaro Cilenti is a Clark Doctoral Fellow of the Clark School of Engineering at the University of Maryland - College Park.

REFERENCES

[1] Eichstädt, S., Elster, C., Esward, T., and Hessling, P., 2010. "Deconvolution filters for the analysis of dynamic measurement processes: A tutorial". *Metrologia,* ***47***, Oct., pp. 522–533.

[2] Eichstädt, S., Wilkens, V., Dienstfrey, A., Hale, P., Hughes, B., and Jarvis, C., 2016. "On challenges in the uncertainty evaluation for time-dependent measurements". *Metrologia,* ***53***(4), June, pp. S125–S135. Publisher: IOP Publishing.

[3] Esward, T., Eichstädt, S., Smith, I., Bruns, T., Davis, P., and Harris, P., 2018. "Estimating dynamic mechanical quantities and their associated uncertainties: application guidance". *Metrologia,* ***56***(1), Nov., p. 015002. Publisher: IOP Publishing.

[4] Nayfeh, A., and Mook, D., 2008. *Nonlinear Oscillations*. Wiley Classics Library. Wiley.

[5] Rijlaarsdam, D., Nuij, P., Schoukens, J., and Steinbuch, M., 2017. "A comparative overview of frequency domain methods for nonlinear systems". *Mechatronics,* ***42***, Apr., pp. 11–24.

[6] Billings, S. A., and Peyton Jones, J. C., 1990. "Mapping non-linear integro-differential equations into the frequency domain". *International Journal of Control,* ***52***(4), Oct., pp. 863–879.

[7] B. Zhang, S. A. Billings, Z. Lang, and G. R. Tomlinson, 2009. "Analytical Description of the Frequency Response Function of the Generalized Higher Order Duffing Oscillator Model". *IEEE Transactions on Circuits and Systems I: Regular Papers,* ***56***(1), Jan., pp. 224–232.

[8] Potter, S. M., 2000. "Nonlinear impulse response functions". *Journal of Economic Dynamics and Control,* ***24***(10), Sept., pp. 1425–1446.

[9] D. Yu, F. Liu, P. Lai, and A. Wu, 2008. "Nonlinear Dynamic Compensation of Sensors Using Inverse-Model-Based Neural Network". *IEEE Transactions on Instrumentation and Measurement,* ***57***(10), Oct., pp. 2364–2376.

[10] Zimmerschied, R., and Isermann, R., 2010. "Nonlinear time constant estimation and dynamic compensation of temperature sensors". *Control Engineering Practice,* ***18***(3), Mar., pp. 300–310.

[11] Vlajic, N., and Chijioke, A., 2015. "Modelling the Response of Force Transducers Under Sine-Sweep Calibration". In IDETC-CIE2015. V008T13A055.

[12] Brunton, S. L., Proctor, J. L., and Kutz, J. N., 2016. "Discovering governing equations from data by sparse identification of nonlinear dynamical systems". *Proceedings of the National Academy of Sciences,* ***113***(15), Apr., p. 3932.

[13] Virtanen, P., Gommers, R., Oliphant, T. E., Haberland, M., Reddy, T., Cournapeau, D., Burovski, E., Peterson, P., Weckesser, W., Bright, J., van der Walt, S. J., Brett, M., Wilson, J., Millman, K. J., Mayorov, N., Nelson, A. R. J., Jones, E., Kern, R., Larson, E., Carey, C. J., Polat, l., Feng, Y., Moore, E. W., VanderPlas, J., Laxalde, D., Perktold, J., Cimrman, R., Henriksen, I., Quintero, E. A., Harris, C. R., Archibald, A. M., Ribeiro, A. H., Pedregosa, F., van Mulbregt, P., Vijaykumar, A., Bardelli, A. P., Rothberg, A., Hilboll, A., Kloeckner, A., Scopatz, A., Lee, A., Rokem, A., Woods, C. N., Fulton, C., Masson, C., Häggström, C., Fitzgerald, C., Nicholson, D. A., Hagen, D. R., Pasechnik, D. V., Olivetti, E., Martin, E., Wieser, E., Silva, F., Lenders, F., Wilhelm, F., Young, G., Price, G. A., Ingold, G.-L., Allen, G. E., Lee, G. R., Audren, H., Probst, I., Dietrich, J. P., Silterra, J., Webber, J. T., Slavič, J., Nothman, J., Buchner, J., Kulick, J., Schönberger, J. L., de Miranda Cardoso, J. V., Reimer, J., Harrington, J., Rodríguez, J. L. C., Nunez-Iglesias, J., Kuczynski, J., Tritz, K., Thoma,

M., Newville, M., Kümmerer, M., Bolingbroke, M., Tartre, M., Pak, M., Smith, N. J., Nowaczyk, N., Shebanov, N., Pavlyk, O., Brodtkorb, P. A., Lee, P., McGibbon, R. T., Feldbauer, R., Lewis, S., Tygier, S., Sievert, S., Vigna, S., Peterson, S., More, S., Pudlik, T., Oshima, T., Pingel, T. J., Robitaille, T. P., Spura, T., Jones, T. R., Cera, T., Leslie, T., Zito, T., Krauss, T., Upadhyay, U., Halchenko, Y. O., Vázquez-Baeza, Y., and SciPy 1.0 Contributors, 2020. "SciPy 1.0: fundamental algorithms for scientific computing in Python". *Nature Methods,* ***17***(3), Mar., pp. 261–272.

[14] Pedregosa, F., Varoquaux, G., Gramfort, A., Michel, V., Thirion, B., Grisel, O., Blondel, M., Prettenhofer, P., Weiss, R., Dubourg, V., Vanderplas, J., Passos, A., Cournapeau, D., Brucher, M., Perrot, M., and Duchesnay, d., 2011. "Scikit-Learn: Machine Learning in Python". *J. Mach. Learn. Res.,* ***12***(null), Nov., pp. 2825–2830. Publisher: JMLR.org.